Computational Analysis of Drag Reduction Methods for a Rearward Facing Step

THESIS

Presented to the Faculty of the Department of Physics and Astronomy
in Partial Fulfillment of the Major Requirements
for the Degree of

BACHELOR OF SCIENCE IN
PHYSICS

Nicodemus Myhre

May 2016

Computational Analysis of Drag Reduction Methods for a Rearward Facing Step

Nicodemus Myhre

Signature of Author:

_____

Department of Physics and Astronomy
May, 2014

Certified by:

_____

Dr. Eric Klumpe
Professor of Physics & Astronomy
Thesis Supervisor

Accepted by:

_____

Dr. Ronald Henderson
Professor of Physics & Astronomy
Chair, Physics & Astronomy

ABSTRACT

The Rearward Facing Step is a classic study of flow separation due to its simplicity and widespread applicability. However, little recent effort has been put into finding spatially compact methods, unlike traditional streamlining, which can significantly reduce the drag associated with this awkward aerodynamic geometry. This study investigates the effect of a rotating cylinder positioned on the corner of the step with the aim of energizing the flow over the step to reduce drag. Specifically, we attempt to determine how changes in the Reynolds number (scale) and specific alterations to the geometry affect the usefulness of the cylinder. This method is both compact and easily simulated. The study is performed computationally using the ANSYS Fluent software package in order to perform tests on a wide variety of scenarios at relatively low cost; however, a real-world verification is underway in a separate research project.

TABLE OF CONTENTS

LIST OF FIGURES

I. INTRODUCTION

The rearward-facing step (RFS) is a classic flow separation study. In this classic study, flow is directed over a sharp right-angled drop. This causes a recirculation region where the boundary layer (BL) is "separated" from the fixed surface. In the recirculation region, the flow is highly turbulent and will even exhibit flow reversal at certain points. A certain distance aft of the step called the "reattachment point", the BL "reattaches" to the surface and recirculation ends. Figure 1 shows typical behavior from three different views.

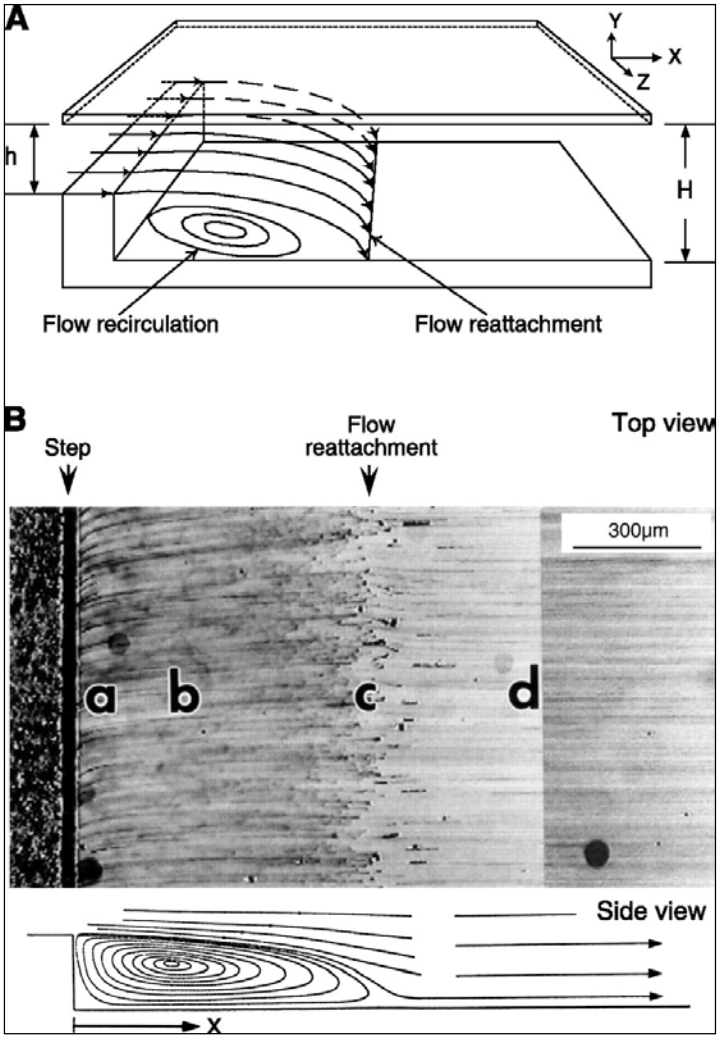

Figure 1: Classic, RFS setup. (Le et al., 1997)

Inevitably, the recirculation region carries with it a great deal of associated drag. This project investigates various methods of alleviating this drag by reducing or eliminating the recirculation region. Among those considered are rounding the corner of the step, mounting a rotating cylinder on the corner of the step, and a stationary flap. However, the focus is on the effects of the rotating cylinder.

The study was performed computationally using the ANSYS FLUENT software package. Indeed, an attempt to investigate so many cases with real-world models would be excessively expensive and time consuming. The computational approach allows us to test a wide variety of geometries, flow speeds, and spin ratios at low cost both in funds and in time. However, due to the fact that computational solutions carry some uncertainties with them, the results will be checked against a real-world verification of a few of the baseline cases which will be performed separate from this study by David G. Rohrer.

While cases such as rounded corners or fillets have been previously analyzed (Bravo & Zheng, 2000; Bao et all, 2003), the use of a rotating cylinder on a RFS has no known documentation in the relevant literature, and is the focal point of this study. If successful, such a method could have applications to drag reduction of vehicles that, for practical reasons, are shaped in ways that are not aerodynamically friendly.

II. BACKGROUND

As mentioned earlier, a great deal of prior investigation has been done on the basic rearward facing step concept (Le et al., 1997; Selimefendigil & Oztop, 2014; Selby, 1983; Gerald, 2000). However, little of this research was done with the purpose of reducing drag. In many cases, the RFS is used specifically to create recirculation to facilitate fuel mixing in RAMJET/SCRAMJET applications. This study is not concerned with such cases, and seeks instead to address the issue of drag reduction when the recirculation associated with a square corner is not desirable. Additionally, the majority of research on the RFS has been performed at high Reynolds numbers (Eklund et al., 1995; Berman et al., 1983; Bravo & Zheng 2000). In this study a wide range of Reynolds numbers (1 – 1,000,000) were investigated to gauge the effectiveness of the proposed method under various circumstances.

III. METHODS

As mentioned previously, the study was performed in the ANSYS Fluent software package. Since a Large Eddy Simulation (LES) has been employed in prior research on the RFS (Fureby, 1999; Akselvoll & Moin, 1996) the same solver scheme was used in this study.

A fundamental aspect of this project was to test the benefits of various drag reduction methods at different values of the Reynolds number R_e. The Reynolds number provides a sense of mathematical scale for a given setup and depends on three parameters of the setup. Equation 1 shows the definition of the Reynolds number.

$$R_e \equiv \frac{v_\infty L}{\nu} \tag{1}$$

In Equation 1, v_∞ is the speed of the oncoming air, L is a reference length, and ν is the kinematic viscosity of the fluid. In our simulations, L and ν were held constant and v_∞ was varied to change the Reynolds number between tests. Thus, for the purposes of this study, R_e and the free stream velocity v_∞ can be treated the same since in all cases they only differ by the same constant factor. The reference length was taken to be the height of the step $L = 4\,ft = 1.2192\,m$, and the kinematic viscosity was the value for air at room temperature $\nu = 1.7894 \times 10^{-5}\,\frac{kg}{m \cdot s}$.

A. Mesh Independence

The study began with the baseline case of a classic RFS at Reynolds numbers ranging from 1 to 1,000,000 in powers of ten. This baseline case was performed three times with meshes of increasing refinement. This gave an indication of the degree to which the choice of mesh was affecting the results. Table 1, shown below, gives the raw results:

	Drag - Cd		
Re	**Mesh #1**	**Mesh #2**	**Mesh #3**
1	37.73	44.12	44.79
10	4.45	4.85	5.01
100	0.91	1.01	0.87
1000	0.26	0.27	0.27
10000	0.36	0.41	0.43
100000	0.39	0.41	0.43
1000000	0.39	0.41	0.42

Table 1: Raw data from mesh independence test

In Table 1, the mesh was progressively refined from Mesh 1 (the lowest resolution) to Mesh 3 (highest resolution). As Table 1 shows, the results did vary slightly between the three meshes. The most notable deviation from the norm was in Mesh 1 at $R_e = 1$. This deviation was concerning enough that Mesh 1 was rejected as an acceptable mesh for future use. The next deviation was seen in Mesh 2 at $R_e = 100$. This variance was not as concerning since fluctuations at this Reynolds number are not uncommon due the fact that the nature of the flow is changing quickly around this Reynolds number. After reviewing the above data, Mesh 2 was chosen as the mesh to be used in all future tests. This was largely due to the fact that Mesh 3 was prohibitively expensive computationally to be used for the large number of future tests planned. Thus, while the results from Mesh 3 may have been marginally better, the results from Mesh 2 were deemed acceptable and Mesh 2 was chosen

for practical reasons. Figure 2 shows the overall behavior of the three meshes, and illustrates the minimal deviation between them. Figures 3-5 show images of the actual meshes.

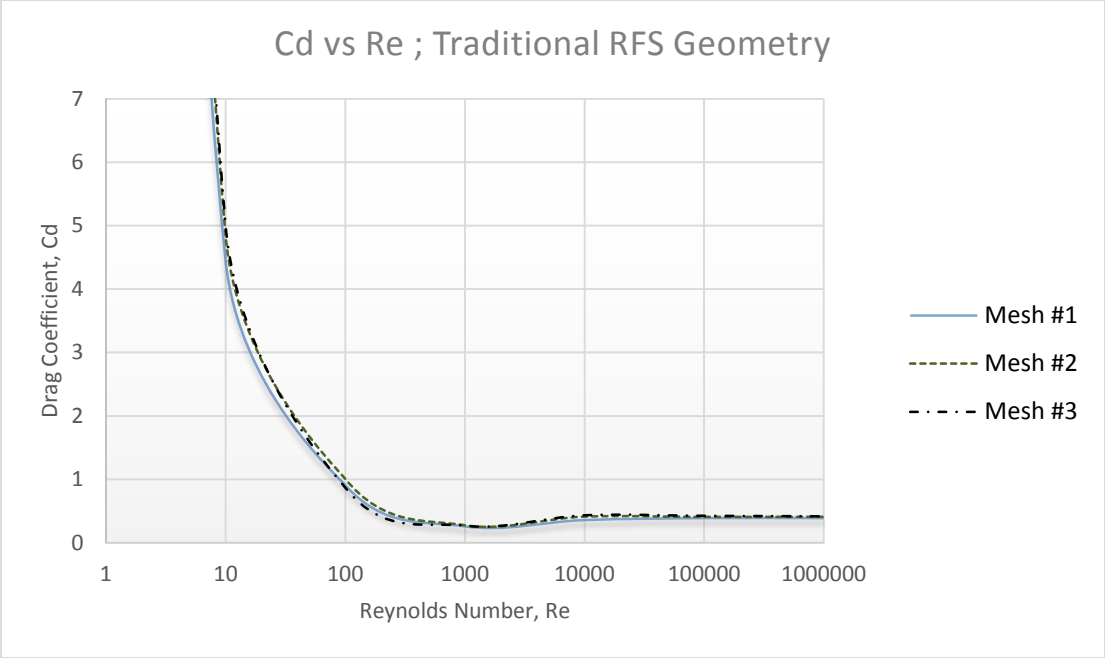

Figure 2: Cd vs Re for mesh independence testing

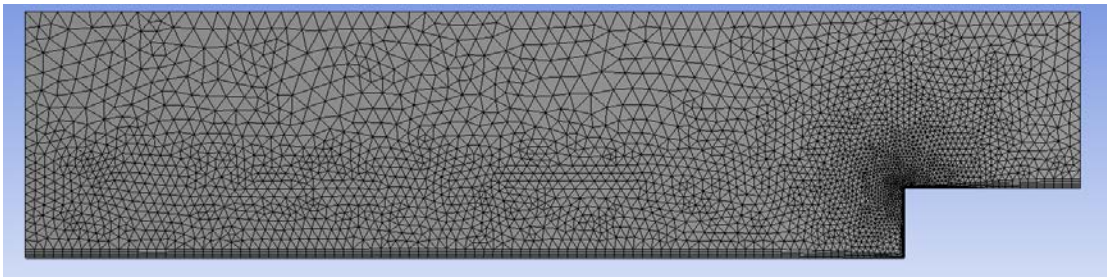

Figure 3: Mesh 1 – Coarse

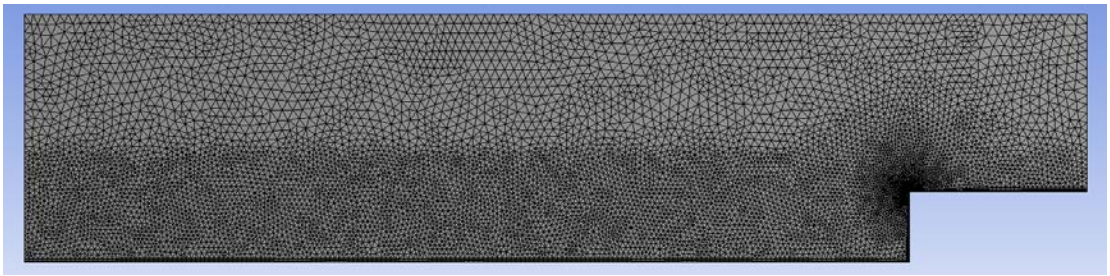

Figure 4: Mesh 2 – Moderate

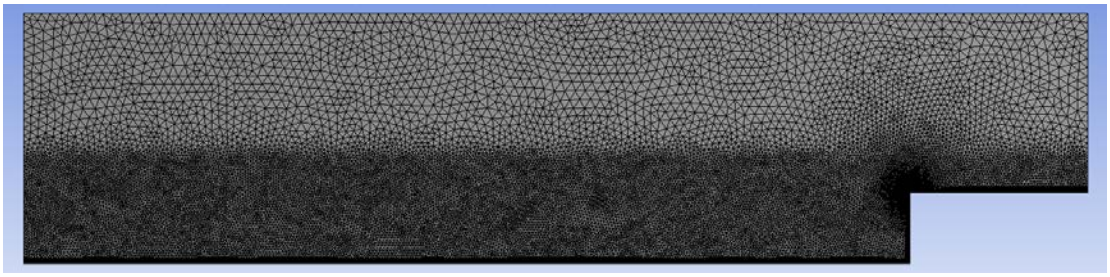

Figure 5: Mesh 3 – Fine

B. Basic Cylinder Step

The cylinder setup modified the traditional RFS setup by installing a cylinder on the corner of the step as shown in Figure 6.

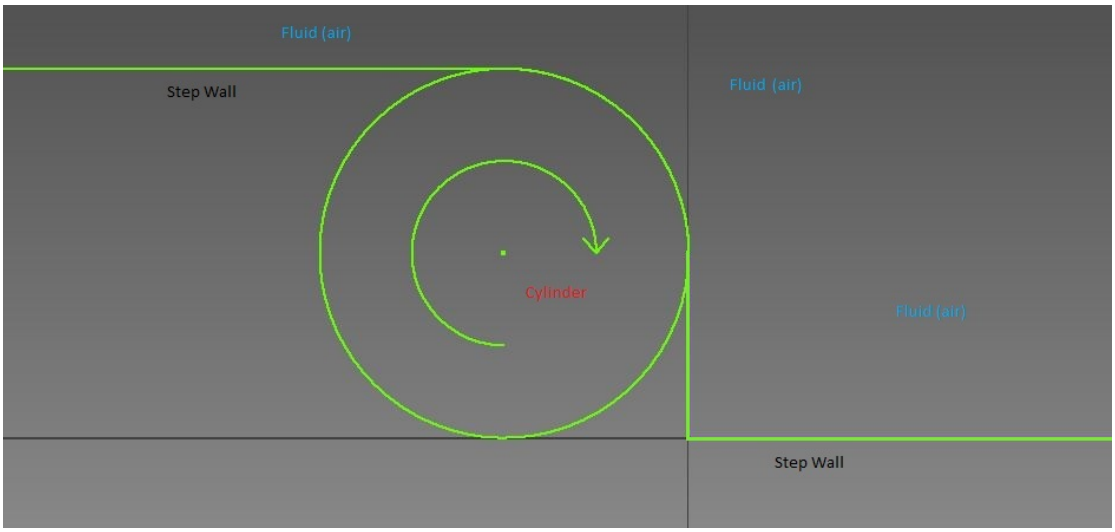

Figure 6: Cylinder setup

This setup was tested with four different values of the spin ratio α ranging from 0 to 2 times the freestream speed, each at the same Reynolds numbers as before. The spin ratio is defined in Equation 2 as the speed of the cylinder's surface divided by the free-stream speed, which is simply the speed of the oncoming air.

$$\alpha \equiv \frac{v_{surface}}{v_{\infty}} \tag{2}$$

Thus, $\alpha = 0$ implies no spin, and $\alpha = 1$ implies that the cylinder's surface speed matches the free-stream speed. These four values of α (0, 0.5, 1, 2) over the seven Reynold's numbers gave a total of twenty eight tests.

C. Stationary Flap

Finally, a stationary flap was mounted on the corner of the step as shown in Figure 7. This case was chosen since it has been used in previous real-world applications for this purpose and serves as a threshold which must be exceeded by the rotating cylinder in order to be practical. As before, this setup was tested across the same seven Reynolds numbers as the cylinder.

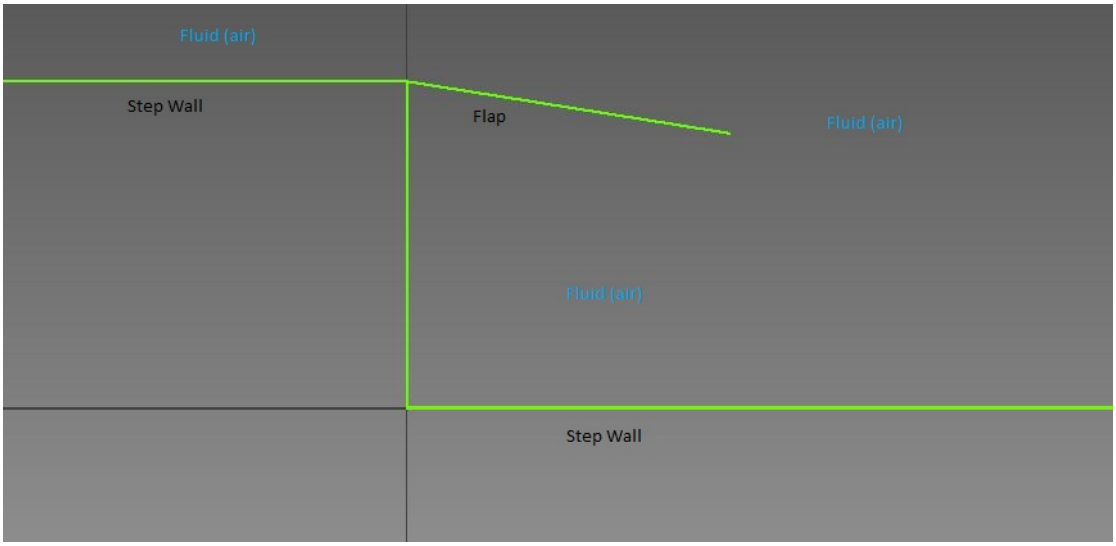

Figure 7: Stationary flap

IV. Results

For the most part, the system behaved as expected. There were some minor anomalies that are discussed below; however, there was a definite tendency for drag to drop across the board as the spin ratio was increased.

Of the slight anomalies in the data, the most unexpected was that the drag coefficient was more heavily affected on a percentage basis at many of the higher Reynolds numbers. Equation 3 shows the nondimensional Navier-Stokes equation (Callender, 2013).

$$\rho^* \frac{D\boldsymbol{V}^*}{Dt^*} = -\boldsymbol{\nabla}^* p^* + \frac{1}{R_e}\mu^* \nabla^{*2}\boldsymbol{V}^* \tag{3}$$

The left side of Equation 3 is the rate of momentum change of the fluid, which Newton's second law tells us will equal net force. The right hand side expresses the net force as the sum of pressure forces, represented by the first term, and viscous forces, represented by the second. Thus, Equation 3 is simply Newton's second law. The asterisks simply mean that the parameters have been nondimensionalized. In the viscous term, we see a factor of $\frac{1}{R_e}$. Thus, the Reynolds number tells us how significant the viscous forces are when compared to the pressure forces. Therefore, as the Reynolds number increases, we expect viscous phenomenon to become less relevant as pressure forces become dominant (Callender, 2013).

Due to the fact that viscous effects become less pronounced as R_e increases, it was anticipated that the flow-energizing effect of the rotating cylinder, which is a distinctly viscous phenomenon, would lose some of its effectiveness as R_e increased.

Figure 8 shows the anticipated type of behavior, where the drag reducing effects fall off with $\frac{1}{R_e}$.

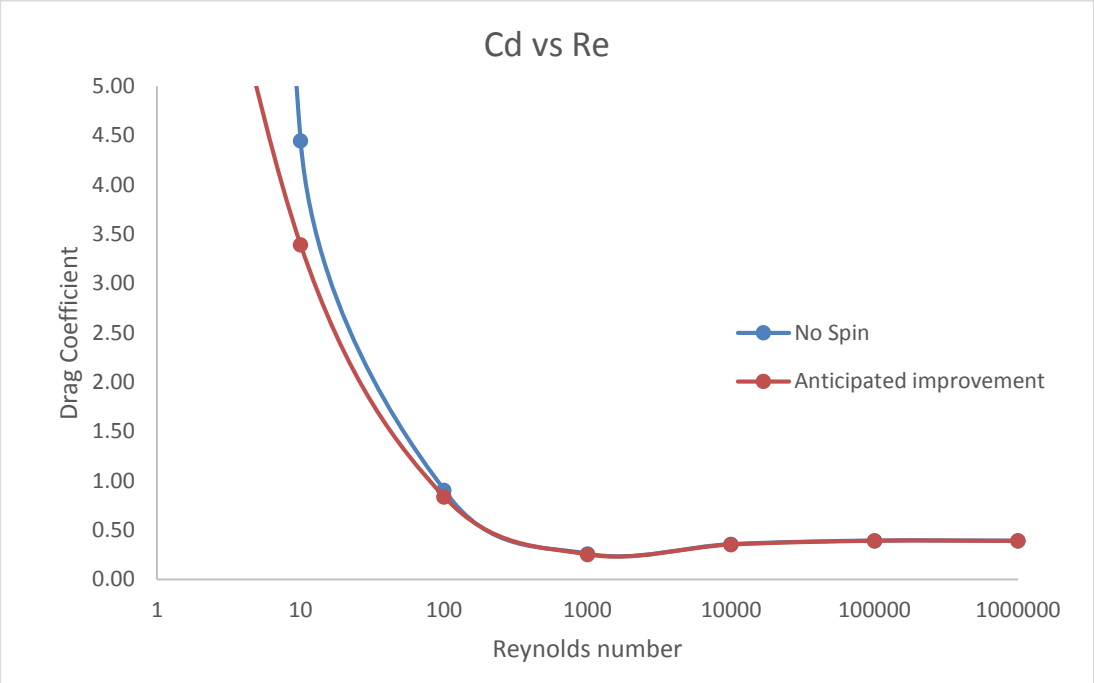

Figure 8: Anticipated improvement from cylinder spin

Surprisingly, the actual behavior was quite different from the expected behavior shown in Figure 8, and significant drag reductions were observed even at the high Reynolds numbers. This unexpected result bodes well for potential real world applications such as the trucking industry where Reynolds numbers are on the order of 10^6, which was the highest R_e in this study.

A. Basic Cylinder

The data for the basic cylinder geometry tests is compiled in Table 2, shown below.

	Cd at Spin Ratio:			
Re	**α = 0**	**α = 0.5**	**α = 1.0**	**α = 2.0**
1	43.29	41.15	40.51	37.84
10	4.73	4.51	4.30	3.92
100	0.82	0.74	0.69	0.62
1000	0.30	0.31	0.32	0.27
10000	0.42	0.37	0.31	0.25
100000	0.36	0.32	0.30	0.29
1000000	0.33	0.31	0.30	0.29

Table 2: Cd vs Re and α - Basic Cylinder

From the raw data, we can quickly see that as a general rule drag decreases as the spin ratio α increases. However, we also see clues of some anomalies that are difficult to visualize. To shed some light on the behavior of the data, the data were plotted in several more accommodating forms.

Figures 9-13 show the raw data in two forms: C_D vs R_e, and C_D vs α. Figure 9 shows the raw data plotted vs R_e.

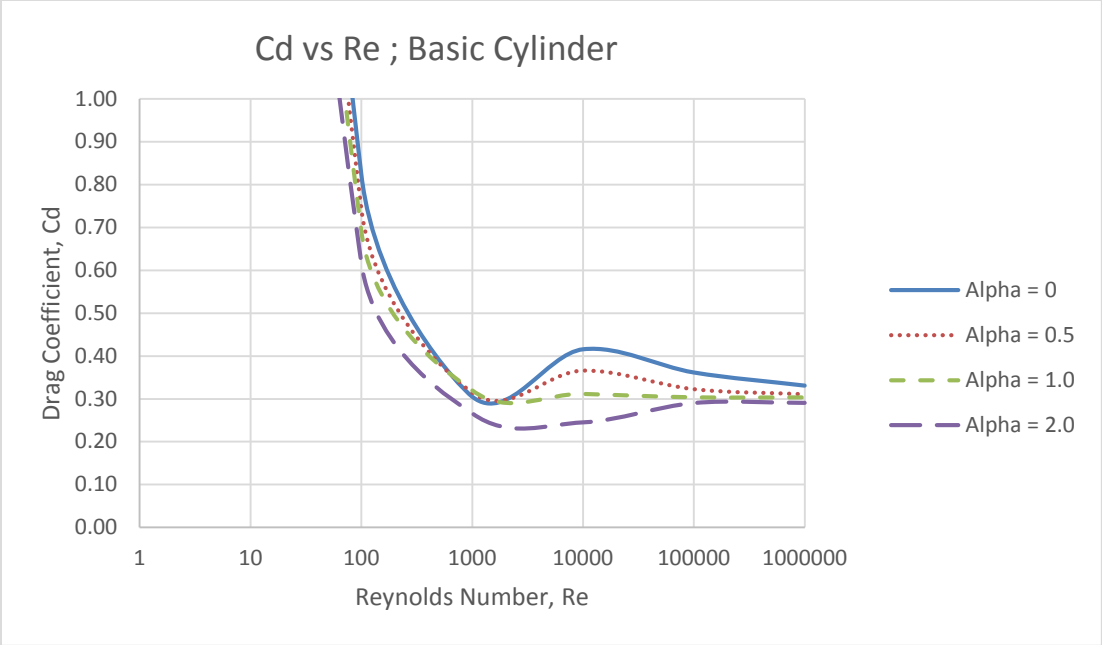

Figure 9: Cd vs Re for constant Spin Ratio

The curves in Figure 9 are similar in shape to the C_D curve for the traditional RFS; however, we can see significant variation already. In particular, the variation at $R_e = 10{,}000$ is quite pronounced. Figures 10-13 plot the data vs. α to show that at all Reynolds numbers, an increase in spin ratio produced a decrease in drag. The only exception to this rule is $R_e = 1{,}000$ (in Figure 13), where a slight increase in drag was observed at $\alpha = 0.5, 1.0$; however, this apparent increase disappeared at $\alpha = 2.0$, when C_D dropped as expected.

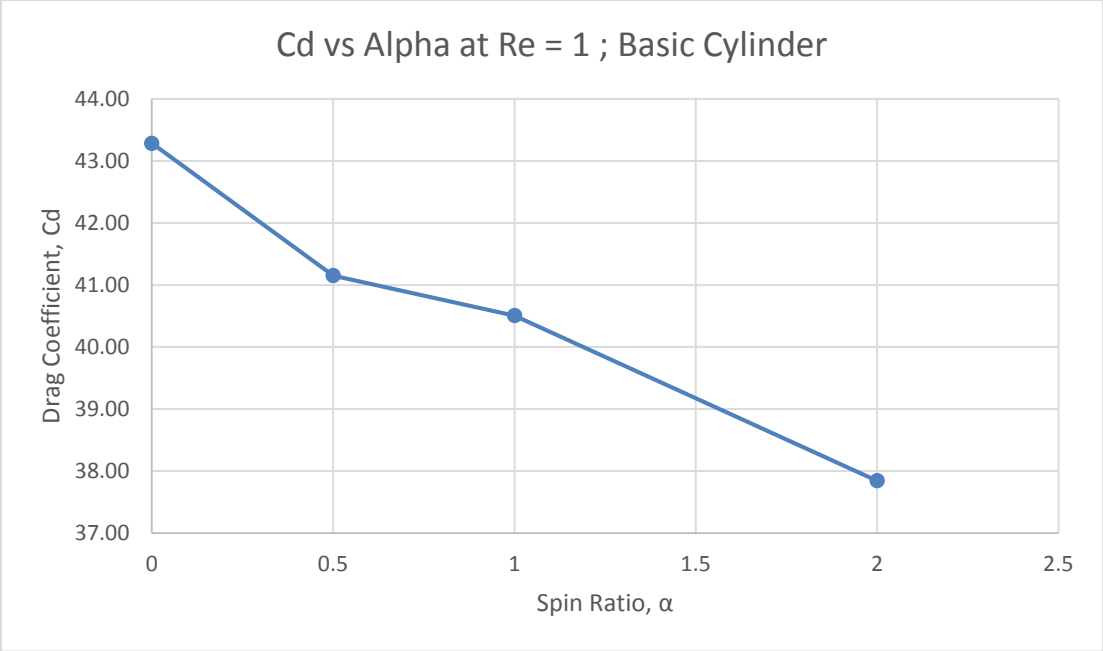

Figure 10: Cd vs Spin Ratio at Re=1

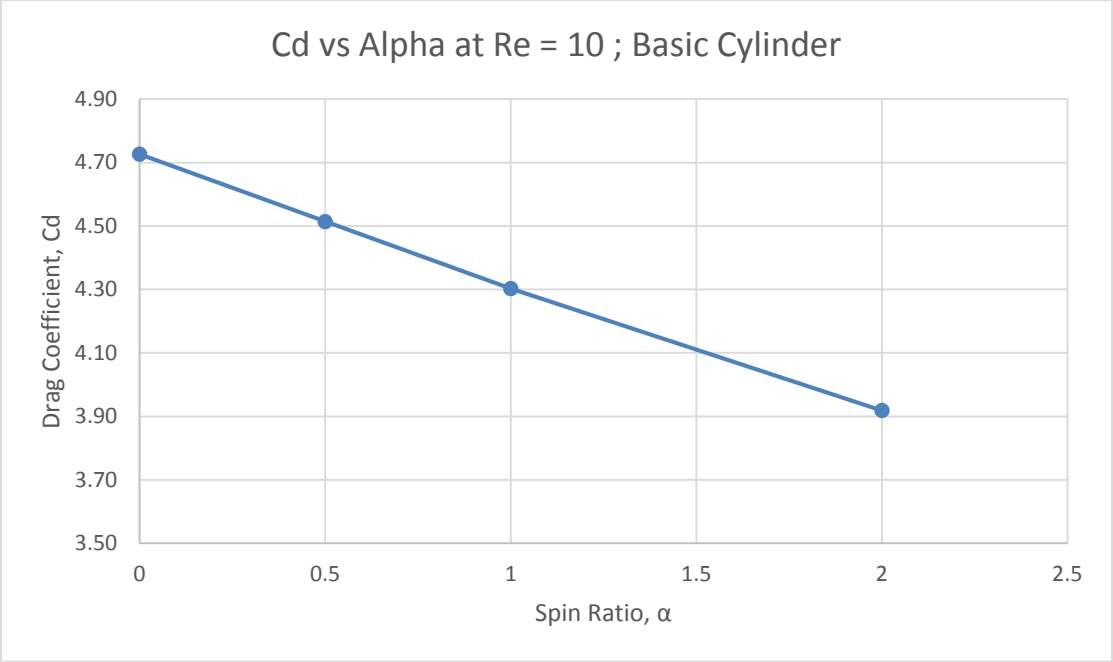

Figure 11: Cd vs Spin Ratio at Re=10

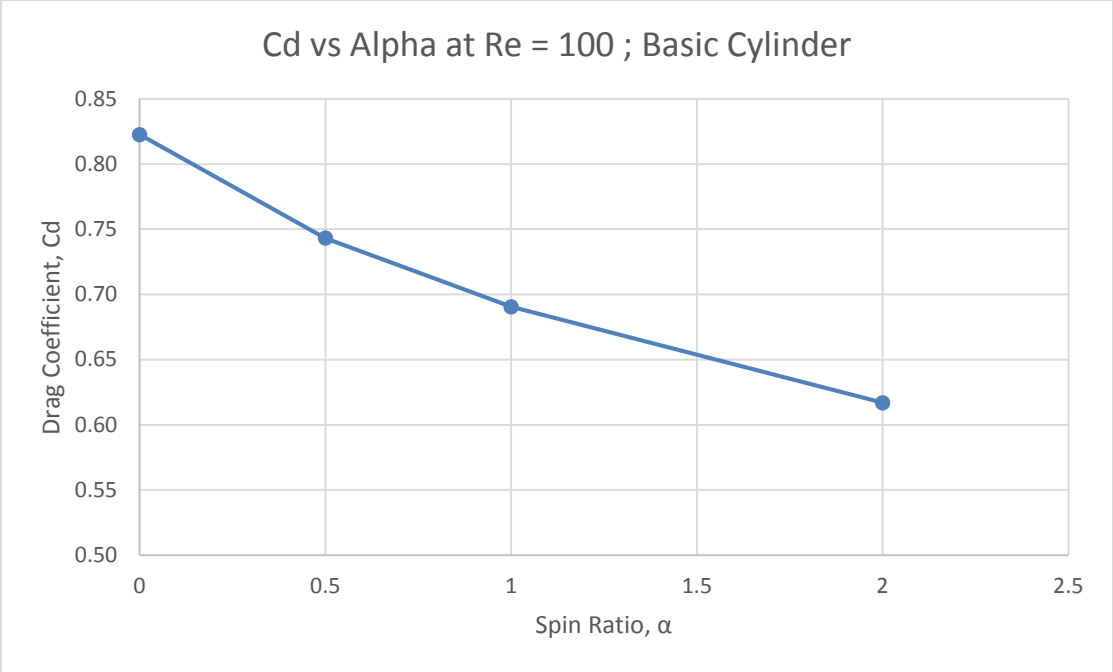

Figure 12: Cd vs Spin Ratio at Re=100

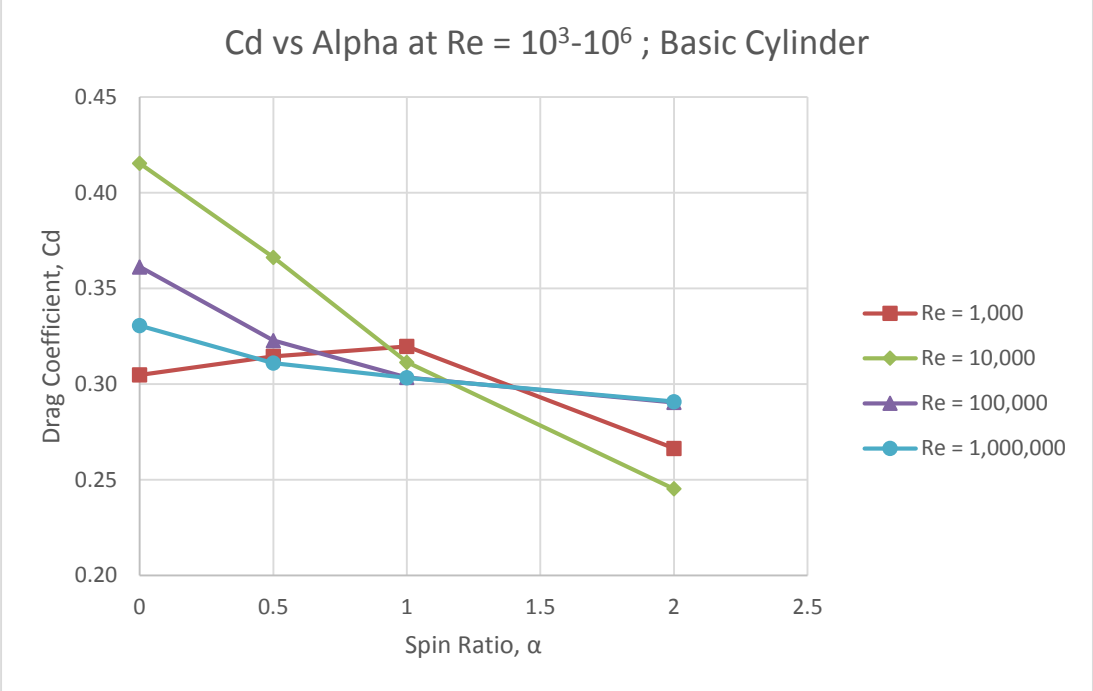

Figure 13: Cd vs Spin Ratio at Re=1,000-1,000,000

Figures 14,15 show the percent change in C_D referenced to the values at $\alpha = 0$. In these two plots (one vs R_e, one vs α), we see that the cylinder had its greatest effect at $R_e = 100$ and $R_e = 10{,}000$. At these two Reynolds numbers, the percent change in C_D took on its most negative values.

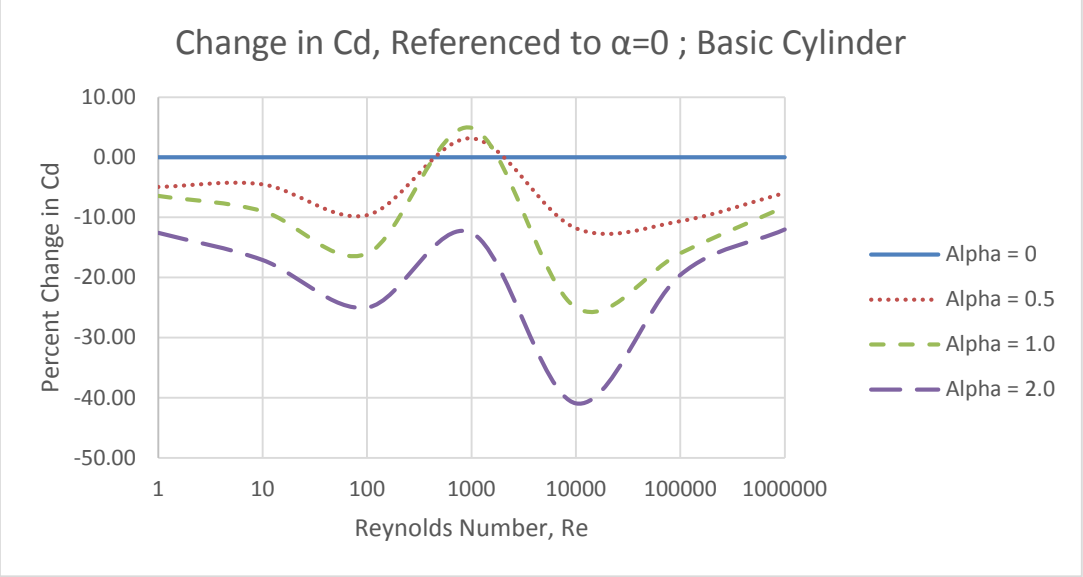

Figure 14: Percent Change in Cd vs Re at constant Spin Ratios

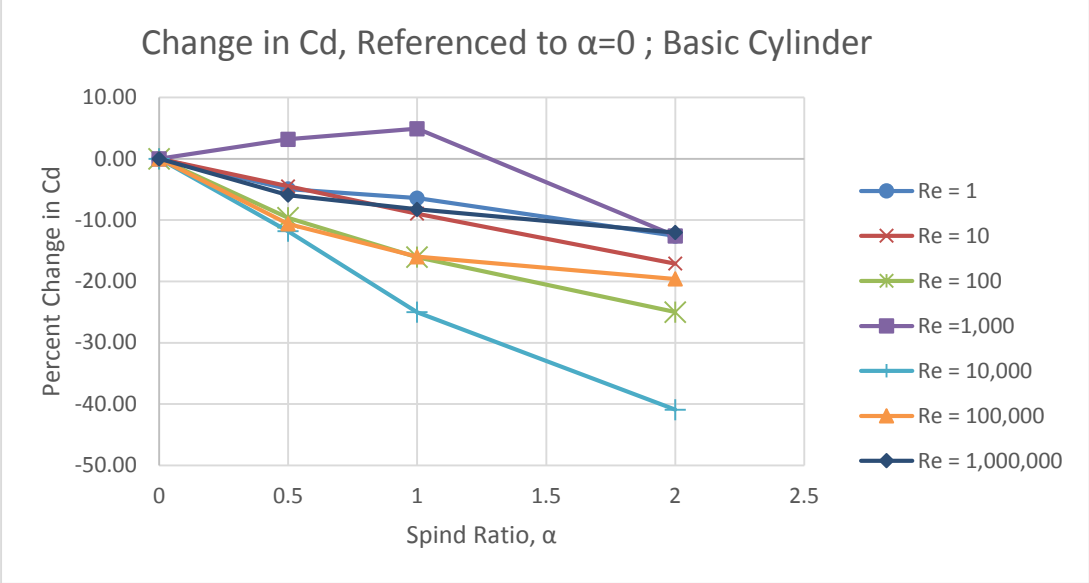

Figure 15: Percent Change in Cd vs Spin Ratio at constant Re

Finally, Figures 16,17 show the percent change in C_D referenced to the traditional right-angled RFS. As before, one (Figure 16) shows curves of C_D vs Re with α constant, and the other (Figure 17) shows curves of C_D vs α with R_e constant. Again, we see the greatest drag reduction (percentage wise) at $R_e = 100$ and $R_e = 10{,}000$.

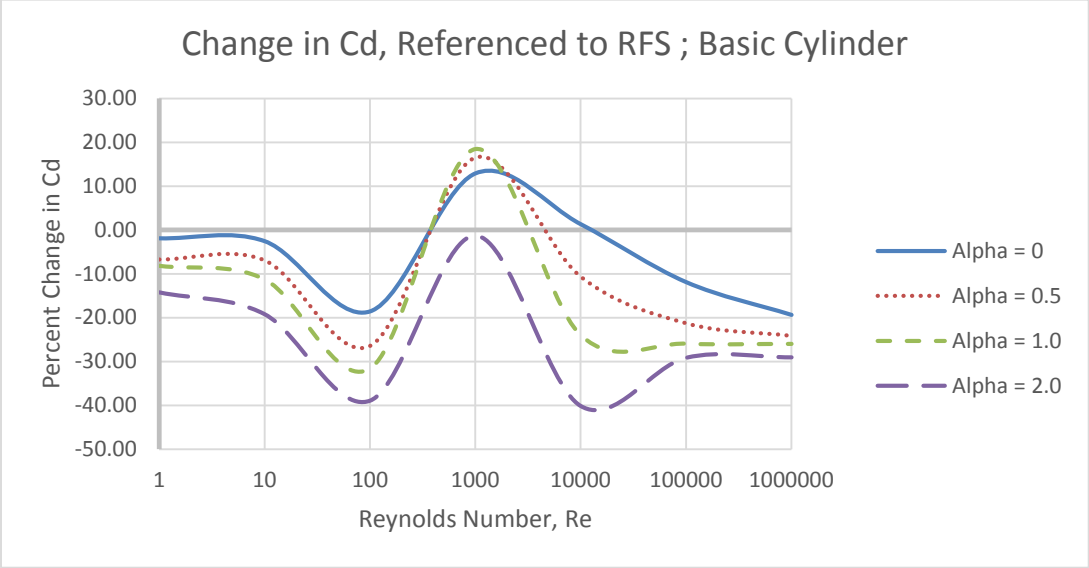

Figure 16: Percent Change in Cd vs Re at constant Spin Ratio

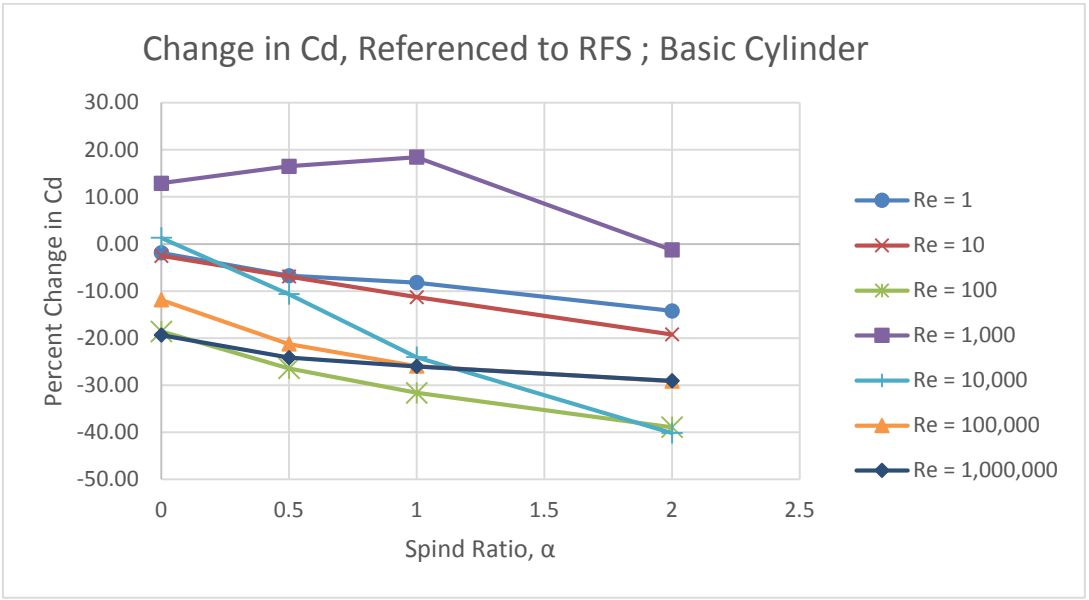

Figure 17: Percent Change in Cd vs Spin Ratio at constant Re

B. Stationary Flap

The data for the simple stationary flap is shown below in Table 3.

Re	Cd
1	69.30
10	5.27
100	0.88
1000	0.32
10000	0.43
100000	0.38
1000000	0.36

Table 3: Cd vs Re for the stationary flap

The raw data on its own shows us nothing new. What we are primarily interested in is how it compares to the previous results. Figures 18,19 illustrate the differences in the same typical representations we have been using this far. From the figures we see that while the stationary flap does outperform the basic step in most instances, and in particular at the high Reynolds numbers, it is consistently outperformed by the cylinder step even with no spin.

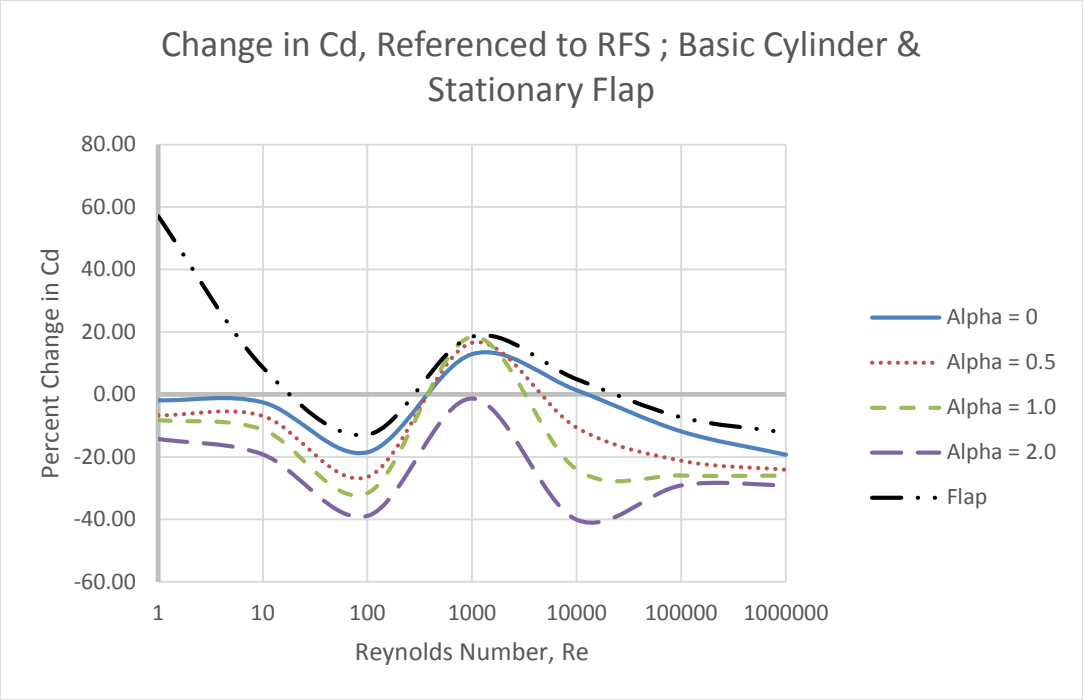

Figure 18: A copy of Figure 16 with the addition of the stationary flap

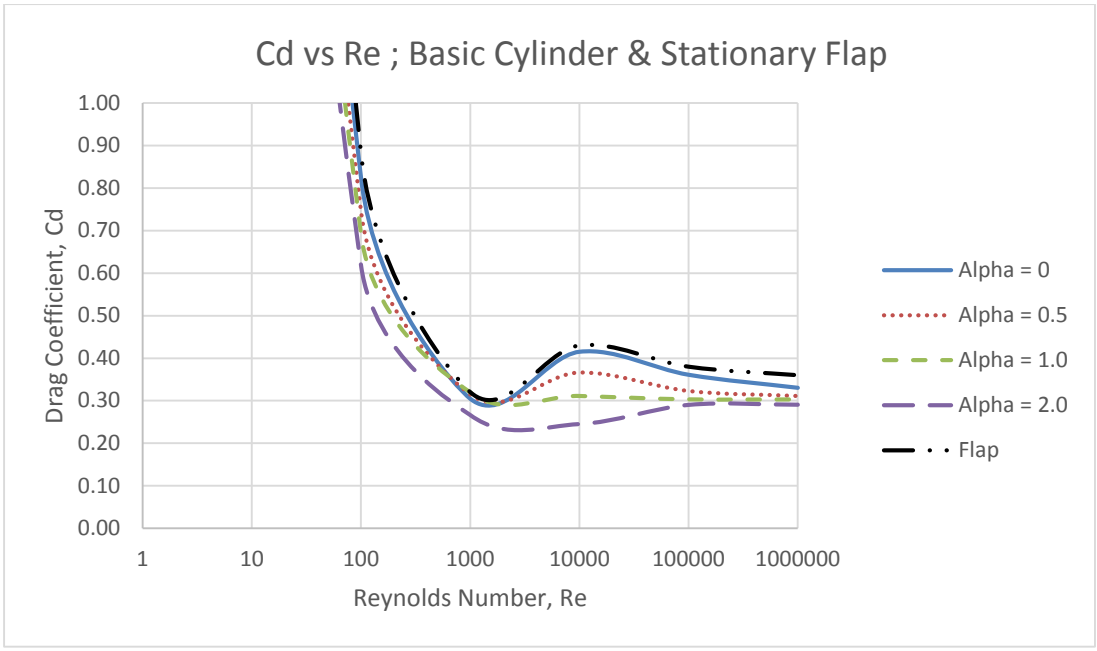

Figure 19: A copy of Figure 9 with the addition of the stationary flap

V. Discussion

The results of this study give us several important insights into the drag characteristics of the RFS. Clearly, there is a point somewhere around $R_e = 1{,}000$ at which the nature of the flow and the drag associated with it are highly unstable. This is no great surprise since it has been observed that it is around these Reynolds numbers that the flow changes from an attached, laminar flow to a separated, turbulent one. Additionally, the drag equation's assumption of quadratic behavior becomes more accurate as we pass this range. The drag equation is shown below in Equation 3.

$$D = \frac{1}{2}\rho v^2 C_D A \tag{3}$$

In the simulation, the density ρ and the reference area A were known constants, v is the free stream velocity which was changed between runs to vary the Reynolds number, and D was computed from a surface integral of both pressure and shear forces in the direction of the flow. With these values in hand, Equation 3 was used to compute C_D. As Equation 3 shows, the drag is assumed to vary with v^2. At low Reynolds numbers, this is not an accurate assumption, and the drag coefficient C_D is forced to pick up the slack. This is what leads to the apparent $\frac{1}{R_e}$ variance of C_D below $R_e = 1{,}000$. However, as the Reynolds number increases and the flow detaches, an assumption of quadratic drag variance becomes quite accurate and C_D takes on a constant value with respect to R_e that is effected only by the geometry of the setup, as shown in all the curves of C_D vs R_e.

Thus, we know there is a fundamental transition of the flow behavior around $R_e = 1{,}000$. Figures 20-25 show velocity contours form the basic RFS to illustrate the transition of the flow as the Reynolds number exceeds $1{,}000$. Unfortunately, no contour image of $R_e = 1{,}000{,}000$ was obtained due to a data loss during the computation. Fortunately, the behavior is not significantly different from that at $R_e = 100{,}000$. In light of this, it is interesting to note that the best drag reductions from the cylinder came in the two Reynolds numbers sandwiching this range: $R_e = 100$ and $R_e = 10{,}000$.

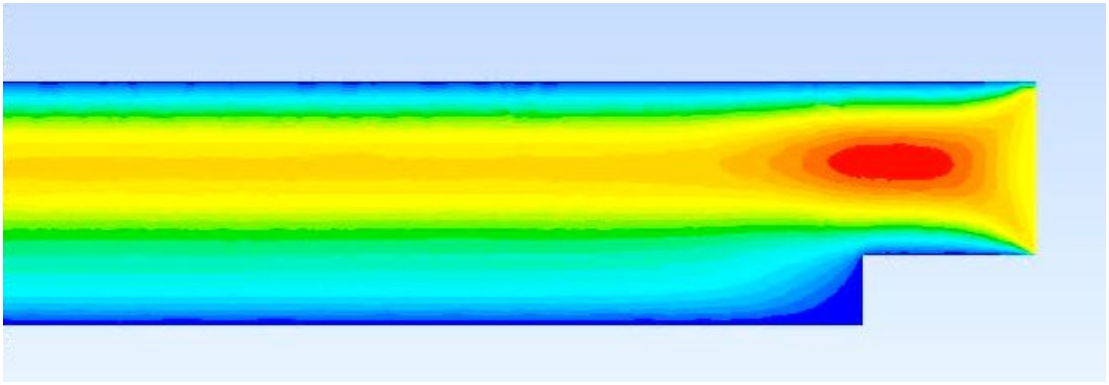

Figure 20: RFS flow behavior at Re = 1

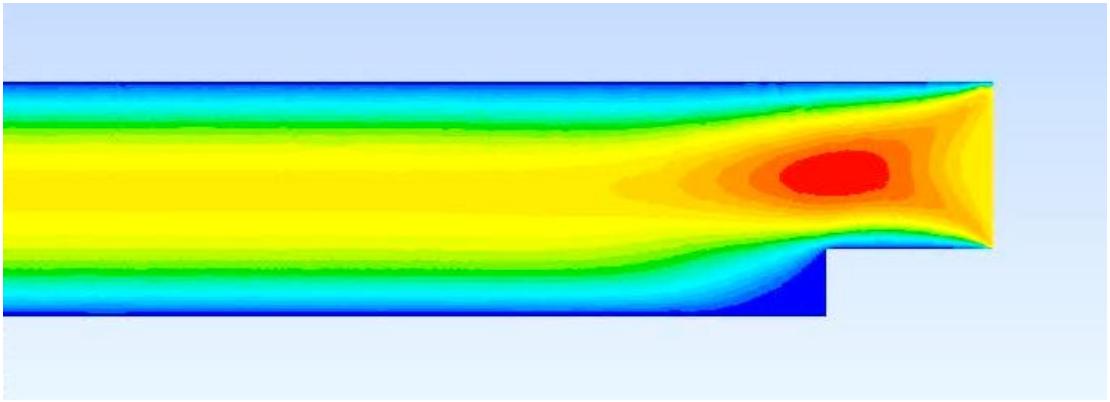

Figure 21: RFS flow behavior at Re = 10

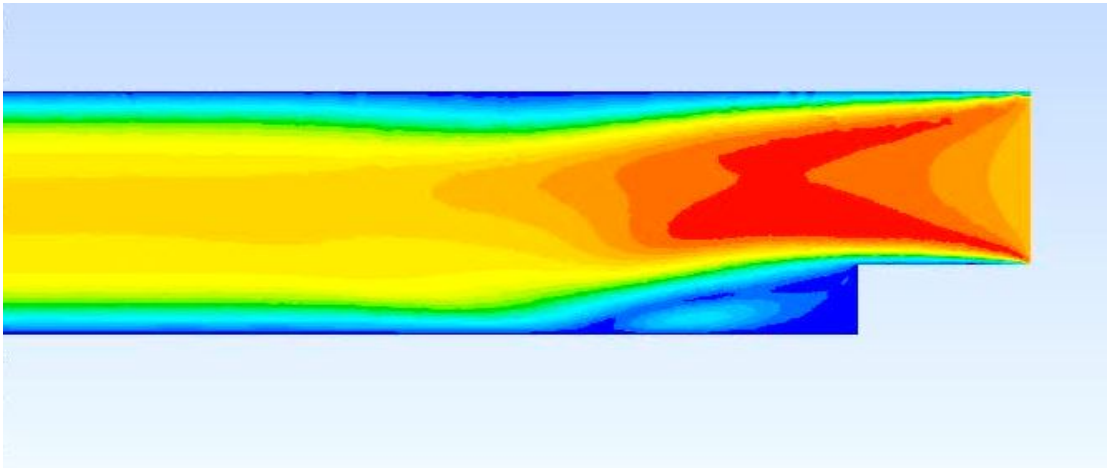

Figure 22: RFS flow behavior at Re = 100

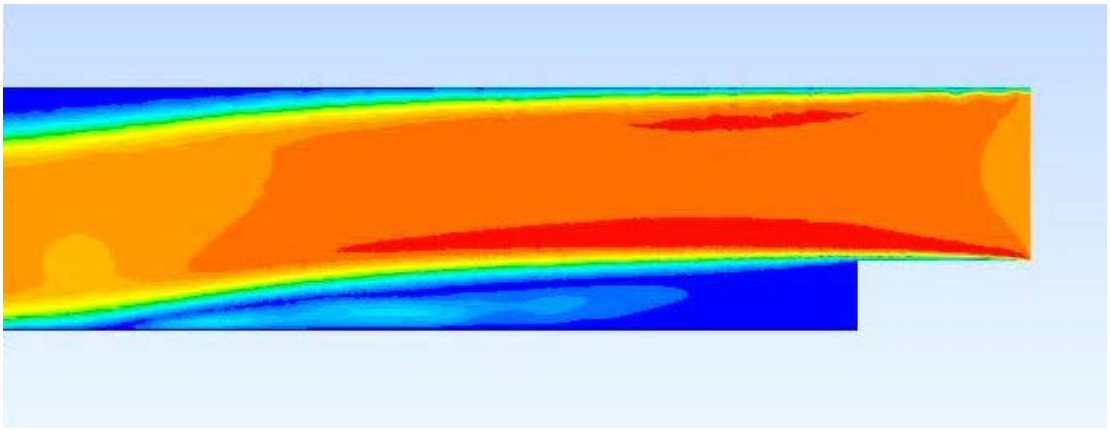

Figure 23: RFS flow behavior at Re = 1,000

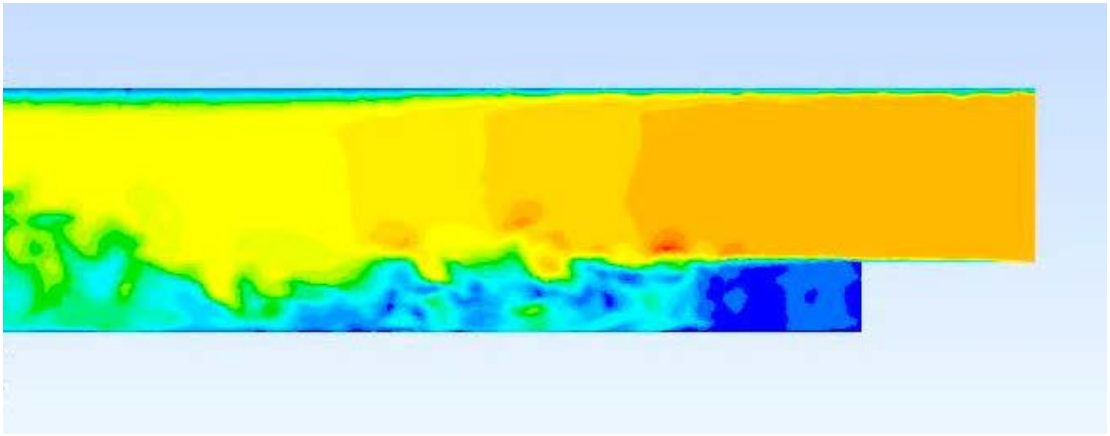

Figure 24: RFS flow behavior at Re = 10,000

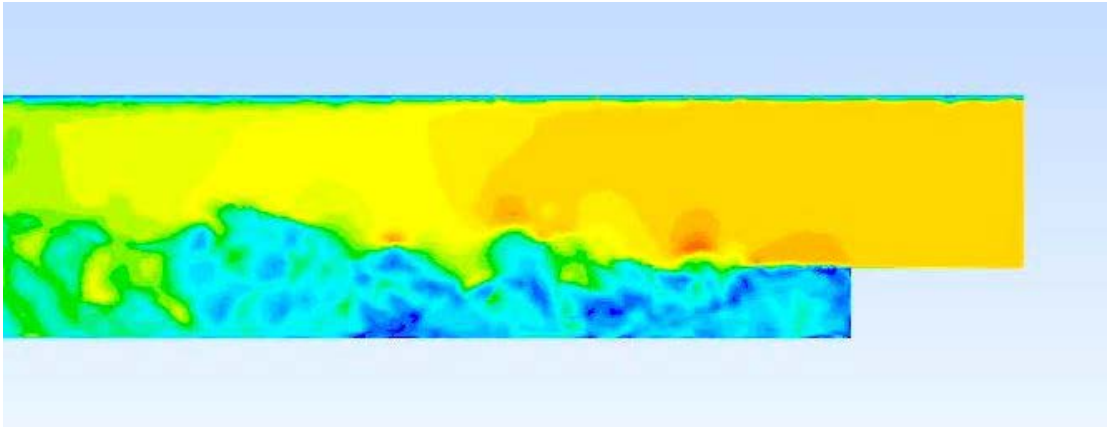

Figure 25: RFS flow behavior at Re = 100,000

First, we recall that the drag reduction at $R_e = 100$ appears for both the cylinder and the simple flap (see Figure 18), although it is notably larger for the cylinder. Since the flow is still laminar, it is no large surprise that the simple flap and the cylinder exhibited similar types of behavior. The primary purpose of the cylinder's spin is to eliminate turbulence; however, if there is no turbulence to begin with, the spin provides only moderate additional help beyond that which comes from simply rounding the corner. Nevertheless, the drag reduction from the cylinder's spin was significant even in this region.

More difficult to explain is the region at $R_e = 1{,}000$, where a slight increase in drag was observed in most cases. This is likely due to the fact that the flow is already in an ideal semi-laminar state, and little room is left for additional improvement. Nevertheless, there is one interesting result in this region. Namely, it appears that at low spin ratios an increase in the amount of spin actually caused an increase in drag. However, this effect went away as α increased to its highest value. The reason for this is difficult to gauge, and will hopefully be clarified by the real-world study mentioned earlier which takes place around this range.

Next, the region of primary interest is that around $R_e = 10{,}000$. Here, the effect of the spin ratio was most pronounced. Fortunately, the explanation of this phenomenon is very straight-forward. As mentioned before, the purpose of the spinning cylinder is to reduce turbulence aft of the step. Typically, the flow transitions from laminar to turbulent around $R_e = 1{,}000$ according to our results; however, as the spin ratio is increased, the onset of this turbulence is delayed such

that the flow is still laminar at higher values of R_e. The faster the spin, the later the flow separation occurred and the greater the drag reduction in this region. This analysis is borne out by the behavior shown in Figure 9, where it is apparent that for higher values of the spin ratio, C_D remains at the low values associated with laminar flow longer. Thus, it is plausible that for values of the spin ratio well in excess of $\alpha = 2.0$ the laminar region could be preserved at much higher Reynolds numbers. This would be particularly useful for many of the proposed applications of the cylinder idea which occur at Reynolds numbers on the order of $R_e \sim 1{,}000{,}000$.

The final region of interest is the Reynolds numbers which are sufficiently high to give turbulent flow. At these Reynolds numbers, the benefits of the cylinder revert back to being similar to those at the low Reynolds numbers. The cylinder is noticeably better than the flap, but not dramatically so. Even so, the reduction is larger on a percentage basis than at the very low Reynolds numbers ($R_e = 1{,}10$).

VI. Conclusion

This study has shown that the rotating cylinder concept consistently outperforms the stationary flap as a method of drag reduction at all Reynolds numbers tested in this study. The effects of the spinning cylinder concept are most pronounced in the region where the cylinder is capable of preventing the flow from becoming turbulent and preserving the low-drag associated with laminar flow. In the future, tests at very high spin ratios may yield the observed dramatic reduction in drag at Reynolds numbers beyond those at which it was observed in the study. Thus, further investigation in this area is warranted. Also, there are significant gaps in the data due to the fact that only Reynolds numbers of integer powers of ten were tested. In particular, regions such as those from $R_e = 100 - 10{,}000$ exhibit rapid changes in the behavior of the cylinder. Thus, future investigation into these regions is warranted. Finally, this study only presents a computational analysis of the RFS, so a real-world verification is currently underway.

VII. REFERENCES

1. Akselvoll, K., & Moin, P. (1996). Large-eddy Simulation of Turbulent Confined Coannular Jets. *Journal of Fluid Mechanics*, 31 5387-411.
2. Berman, H.A., Anderson, J.J., & Drummond, J.P. (1983). Supersonic flow over a rearward facing step with transverse nonreacting hydrogen injection. *AIAA Journal*, 21 1707-1713.
3. Bravo, H. and Zheng, Y. (2000). Turbulent Flow over Step with Rounded Edges: Experimental and Numerical Study. *J. Hydraul. Eng.*, 126(1), 82–85.
4. Callender, M. N. (2013). Ph.D. dissertation. Univertisy of Tennessee. A Viscous Flow Analog to Prandtl's Optimized Lifting Line Theory Utilizing Rotating Biquadratic Bodies of Revolution. Retrieved from Trace: Tennessee Research and Creative Exchange.
5. Eklund, D., Fletcher, D., Hartfield, R., Northam, G., & Dancey, C. (1995). A Comparative Computational Experimental Investigation of Mach-2 Flow Over a Rearward-Facing Step. *Computers & Fluids*, 24(5), 593-608.
6. Fatih Selimefendigil and Hakan F. Oztop (2014). Control of Laminar Pulsating Flow and Heat Transfer in Backward-Facing Step by Using a Square Obstacle. *Journal of Heat Transfer*, Vol 136, Iss 8.
7. Feng Bao, Uwe Dallmann (2003). Some Physical Aspects of Separation Bubble on a Rounded Backward-Facing Step. *Aerospace Science and Technology*. Vol 8, Iss 2, p83-91. Retrieved February 13, 2015 from www.sciencedirect.com.

8. Fureby, C. (1999). Large Eddy Simulation of Rearward-Facing Step Flow. *AIAA Journal*, *37*(11), 1401.
9. Gerald C., L. (2000). Scaling of turbulent wall pressure fluctuations downstream of a rearward facing step. *The Journal Of The Acoustical Society Of America*, *107*(1), L1.
10. Hung Le, Parviz Moin, and John Kim (1997). Direct Numerical Simulation of Turbulent Flow Over a Backward-Facing Step. *Journal of Fluid Mechanics*, 330, pp 349-374 doi:10.1017/S0022112096003941
11. Selby, G. V. (1983). Applicability of the independence principle to subsonic turbulent flow over a swept rearward-facing step. *AIAA Journal*, 21 1603-1604.